Article

The Wind Profile Characteristics of Super Typhoon Lekima Based on Field Measurement

Yanru Wang [1], Qianqian Qi [2], Shuqin Zheng [3,*], Bin Fu [1], Maoyu Zhang [1], Xu Wang [4], Chuanxiong Zhang [3] and Lei Zhou [4]

1   School of Civil Engineering, Taizhou University, Jiaojiang 318000, China; yanrupiaoyang@163.com (Y.W.); dorofubin@tzc.edu.cn (B.F.) ryanzmy0577@tzc.edu.cn (M.Z.)
2   School of Civil Engineering, Xinyang University, Xinyang 464000, China; 622200970065@mails.cqjtu.edu.cn
3   Key Laboratory of Intelligent Lifeline Protection and Emergency Technology for Resident Aty, Wenzhou University of Technology, Wenzhou 150080, China; zhangcx@wzu.edu.cn
4   State Key Laboratory of Mountain Bridge and Tunnel Engineering, Chongqing Jiaotong University, Chongqing 400074, China; xuwang@cqjtu.edu.cn (X.W.); lixuezl@tju.edu.cn (L.Z.)
*   Correspondence: zhengshuqin@wzut.edu.cn

Abstract: Many cities in coastal areas are prone to typhoon disasters due to their location on the Pacific storm path, and the direct effect of catastrophic winds can lead to the destruction of low-rise buildings and severe damage to high-rise structures. The purpose of this study was to enhance the understanding of boundary layer wind profiles of strong typhoons in coastal areas and reduce property losses and casualties caused by wind disasters. Based on the field measurements of wind profile acoustic radar in coastal areas, the variation characteristics of the boundary layer wind profile during the passage of super typhoon Lekima were first studied in depth, and the evolution law of the typhoon boundary layer profile was summarized. Then, the effects of typhoon horizontal structure, topography, wind speed, and time distance on the characteristics of the typhoon profile were discussed, respectively. Finally, the evolution characteristics of wind profile parameters were obtained by fitting three wind profile theoretical models. Due to the strong variability of typhoon profile morphology, the theoretical model of wind profile is only applicable to the wind profile from the bottom to the low-level jet height of typhoons, while wind parameters are closely related to the spatial location of the typhoon wind field.

Keywords: strong typhoon; wind profile; evolution; wind parameters; field measurements

1. Introduction

The evolution of average wind speed within the atmospheric boundary layer with vertical altitude has always been a hot topic in structural wind resistance research. With the emergence of modern towering buildings, their structural shapes have become increasingly complex. Strong typhoons can seriously damage building structures, affecting their usability and durability. Studying the characteristics of typhoon wind fields, especially mastering the characteristics of typhoon profiles and their influencing factors and the evolution laws of related wind parameters, can further avoid the vibration and even damage of tall wind-sensitive structures under wind load excitation, thereby improving the safety and economy of high-rise building design [1].

Due to the high temperature of the ocean surface in tropical areas and the large amount of sea water evaporation, it is easy to form a low-pressure center dominated by the upwind. The low-pressure center gradually moves and strengthens with the rotation of the earth, thus driving more airflow around the deflection and forming a regular rotation of tropical cyclones. When the wind force near the bottom center of a tropical cyclone reaches 12 (32.7 m/s), it is considered a typhoon. The typhoon profile is related to topography, atmospheric humidity, surface roughness, atmospheric stability, Coriolis force, and other

factors. Wind engineers have studied wind field characteristics through methods such as field measurements [2,3], numerical simulations [4,5], and wind tunnel tests [6,7].

As the most direct and effective way, field measurement is often used by scholars to study typhoon wind characteristics. Franklin [8] studied the wind profile characteristics of 17 hurricanes in the eye wall area and the outer circulation area by using GPS dropsonde. It was found that the hurricane eyewall area had higher wind speeds, and the maximum wind speed in the outer circulation area occurred at a height of 1 km. Powell et al. [9] found that the average wind speed in a tropical cyclone profile increases logarithmically with altitude, with the maximum value occurring at 500 m. Based on the measured data of gradient mast towers, Song et al. [10,11] found that the characteristics of typhoon wind profile were significantly different from those of good wind profile. Lin et al. [12] studied the wind speed profile and related parameters in typhoon-prone areas along the southeastern coast of China. They found that the wind profile index before the typhoon eye passed was higher than that after the typhoon eye passed, while the roughness length was the opposite. He et al. [13] studied the downwind profile characteristics of typhoons with different ground roughness based on a 356-m meteorological gradient tower. In fact, normal winds with high Beaufort scales also occur frequently. Liu [14] analyzed the average wind speed and wind direction profiles of 16 strong wind days based on a wind profiler and believed that the wind resistance design of super high-rise buildings should mainly consider Class I.

Real-time monitoring of meteorological satellites also plays a crucial role in typhoon research [15]. It can monitor and track the location and movement path of typhoons in real-time, collect key meteorological data, and provide valuable information for studying and improving typhoon prediction models [16–18]. With the development of computer technology, numerical simulation is widely used in wind research. For example, large eddy simulation (LES) is used to simulate turbulence [19]. Ren et al. [20] used CFD and LES to simulate the spatial wind field and turbulence of complex terrain and established a spatial wind field prediction model. The WRF model has been widely used in typhoon wind field simulation in recent years [21,22]. Zhang [23] used the WRF-UCM coupling model to simulate the urban wind field during the landfall of a strong typhoon. Due to the complexity and randomness of wind, the lack of observation data in East Asia and the low spatial and temporal resolution of data, the study of wind characteristics still has various obstacles and is difficult to master [24]. There are few studies on the characteristics and evolution of typhoon low-level jet [25]. More importantly, the existing research mainly focuses on the observation of 100-m height, which makes it difficult to reflect the real wind profile of the typhoon boundary layer, and there are few systematic studies on the characteristics of disaster-causing wind profile and its influencing factors [26].

In this study, the profile characteristics of super typhoon Lekima were studied in depth based on the measured data of ultra-efficient and long-distance wind profile acoustic radar in the coastal area of Taizhou, Zhejiang Province, China. The evolution law of the vertical distribution of wind speed in the atmospheric boundary layer under different influence stages of strong typhoons was systematically analyzed. The factors affecting the profile characteristics and the evolution law of related wind parameters were explored. It was intended to enhance the understanding of the profile characteristics of the boundary layer under strong typhoons in coastal areas, to provide a reference for typhoon boundary layer simulation, and to promote the wind resistance design of high-rise wind-sensitive buildings in coastal areas. This has important significance for the wind resistance design of civil engineering structures and disaster prevention and reduction.

2. Overview of Field Measurements

2.1. Measured by Typhoon Lekima

Super typhoon Lekima formed over the western North Pacific Ocean at 2:00 Beijing time on 4 August 2019, and moved northwestward. At 1:45 on the 10th, it made landfall along the coast of Cheng Nan Town, Wenling City, Zhejiang Province, China, with a maximum wind speed of 52 m/s near the center of the bottom layer and a minimum

pressure of 930 hPa. Lekima is the third strongest typhoon to land in East China in nearly 70 years. Due to its long duration and wide range of disaster impacts, on 30 April 2021, the Typhoon Committee decided to remove the name of super typhoon Lekima and replace it with the new typhoon name "Co-may".

Figure 1a is the optimal track map of typhoon Lekima provided by the China Meteorological Administration. Figure 1b is the wind profile acoustic radar from the measured data source of this study, and Table 1 shows the detailed parameters of the instrument. Wind profile acoustic radar can continuously measure the distribution characteristics of atmospheric wind speed, wind direction, and disturbance in the vertical range of 30–950 m with ultra-high efficiency and long-distance continuous measurement, and can provide horizontal wind components updated every minute, including average wind speed per minute, standard deviation of average wind direction and air volume, temperature, signal-to-noise ratio, turbulence intensity in wind energy applications, stability in air quality applications, etc. It probes 47 height layers at 20 m intervals in a vertical range of 30–950 m.
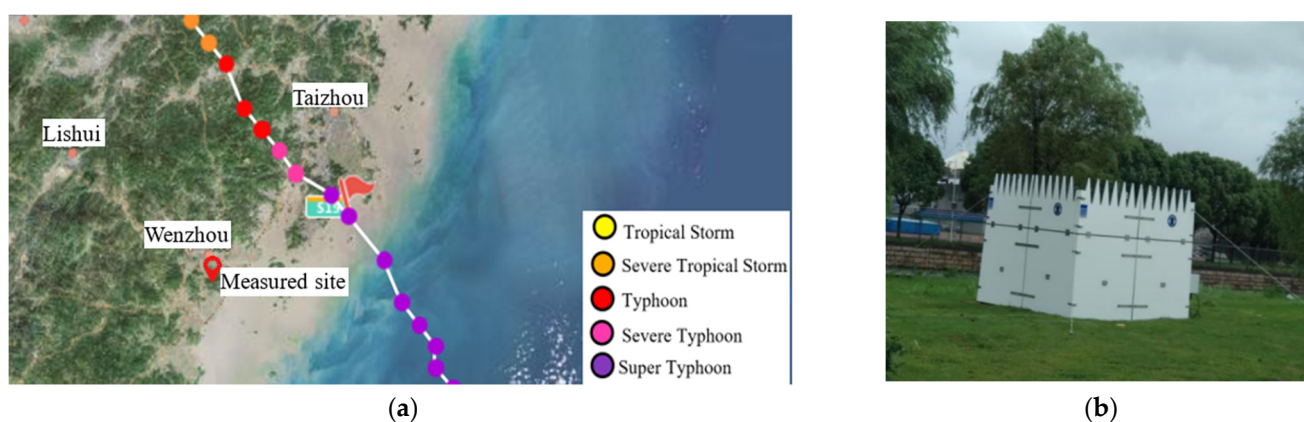

(a)   (b)

Figure 1. Best track of typhoon and the Sodar Wind Profiler, including (**a**) Lekima (in CST, or UTC + 8). The tropical cyclone intensity scale from China Meteorological Administration: Tropical Depression (10.8–17.1 m/s); Tropical Storm (17.2–32.6 m/s); Typhoon (32.7–61.2 m/s); Super Typhoon (61.2 m/s); (**b**) The Sodar Wind Profiler.

Table 1. Specifications of the Sodar Wind Profiler.

Parameter	Value
Beamwidth	$0°, \pm22°, \pm29°$
Vertical resolution	10 m
Minimum measurement height	20 m
Maximum measurement height	1000 m
Sampling period	60 s
Horizontal wind speed accuracy	0.1~0.3 m/s
Vertical wind speed accuracy	0.03~0.1 m/s
Wind direction accuracy	$1.5°$
Horizontal wind speed range	0~50 m/s
Vertical wind speed range	−10~10 m/s

2.2. Measurement Location and Sample Selection

2.2.1. Measured Site

The measurement site is located in the northern campus of Wenzhou University, Ouhai District, Wenzhou City, Zhejiang Province, which belongs to the southeastern coastal area with many bays. The topography of the measurement point and its surrounding area is shown in Figure 2. About 2 km east of the measured point is Daluo Mountain, with the highest altitude of 707.4 m. The southeast side is about 17 km away from the coastline of the East China Sea, where a large number of typhoons land or pass through every year. The

northeast side has the second largest river in Zhejiang, the Oujiang River; the northwest side is the open Sanyang wetland, and the west side is the urban area of Wenzhou, which belongs to the suburbs of the city. The distance between the typhoon landing site and the observation point is about 82 km. During the typhoon period, at 3:00 on 10 August 2019, the observation point is the closest distance from the typhoon center, about 70.8 km, and the intensity level of the typhoon is a strong typhoon at this time.
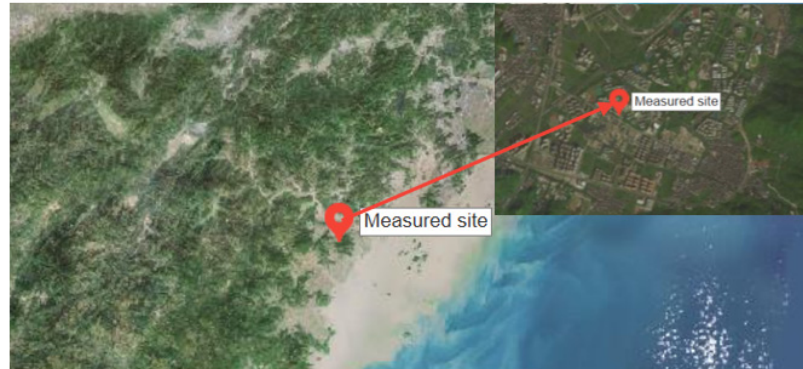

Figure 2. The measured site and surrounding terrain.

2.2.2. Sample Selection

The measured typhoon data started of the Lekima generation, from 14:00 on 4 August 2019, to 14:00 on 13 August 2019, in China Standard Time (CST = UTC + 8 h), totaling 216 h. The observation time interval was 1 min, and the average time interval was processed according to 10 min. Considering the time and space factors, a total of 1,192,320 wind speed and wind direction samples were collected. Some data obtained by remote sensing equipment have low quality and cannot be used for any analysis. To ensure the reliability and scientific validity of the analysis results, it is necessary to remove outliers and missing data. Due to the large sample size of the total observed data, invalid samples are scattered among valid samples, and the elimination of invalid samples in data processing does not affect the overall reliability and credibility of the data. In the subsequent calculation and analysis process of this paper, the invalid samples were excluded and only the valid samples were studied.

3. Measured Data Processing

The vertical distribution of wind speed in the atmospheric boundary layer is an important theoretical basis for the wind-resistant design of high-rise buildings in coastal areas. In this study, three commonly used wind profile theoretical models were used to analyze the global profile characteristics of super typhoon Lekima.

3.1. Theoretical Model of Wind Profile

3.1.1. Log-Law Model

Considering the flow characteristics of the atmospheric boundary layer and under neutral atmospheric stability conditions, the expression for the wind profile log-law model can be derived from the solution of the average wind speed differential equation [27]:

$$u(z) = \frac{u_*}{\kappa} \ln \frac{z}{z_0}$$

where, z_0 is the roughness length, u_* is the friction velocity, κ is the von-Kármán constant, generally 0.4, and $u(z)$ is the wind speed at the vertical height z.

According to the Monin–Obukhov similarity theory [28], when the atmosphere is in a stable or unstable state, the wind profile can be described in a more general form by adding a correction function:

$$u(z) = \frac{u_*}{\kappa}\left[\ln\frac{z}{z_0} + \psi\left(\frac{z}{L}\right)\right]$$

where, ψ is the Monin–Obukhov function and L is the Monin–Obukhov length. $\psi(z/L)$ has different values under different atmospheric stability conditions, and 0 is taken in the case of neutral stratification. Under neutral stratification, Equation (1) is a widely used wind speed profile expression, which is widely used in the field of micrometeorology because of its good theoretical basis and experimental support, and can better describe the wind profile in the near-surface range.

3.1.2. Power-Law Model

By analyzing wind speed data with different ground roughness in cities, open grasslands, and rural areas, Davenport [29] pointed out that the change of horizontal average wind speed with height satisfies the exponential function. Research has shown that the power law model can satisfy the wind profile characteristics in various terrains and has a simple expression [30,31]. This model is widely adopted in standards of the United States, China, and Japan [32–34]:

$$u(z) = u(z_1)\left(\frac{z}{z_1}\right)^{\alpha}$$

where, $u(z)$ and $u(z_1)$ are the wind speed at altitude z and reference height z_1, respectively, and α is the wind profile index, which is related to altitude, topography, horizontal wind speed, and atmospheric stratification, representing the change law of wind speed with the increase or decrease of altitude. A positive value indicates compliance with the power law model, while a negative value suggests that the change of wind speed with vertical height deviates from the power law profile.

3.1.3. Deaves-Harris Model

Deaves and Harris [35] proposed an improved wind profile model based on the logarithmic law model by introducing the atmospheric boundary layer height and fully considering the influence of ground roughness:

$$u(z) = \frac{u_*}{\kappa}\left[\ln\frac{z}{z_0} + 5.75\frac{z}{h} - 1.88\left(\frac{z}{h}\right)^2 - 1.33\left(\frac{z}{h}\right)^3 + 0.25\left(\frac{z}{h}\right)^4\right]$$

where, h is the height of the boundary layer, and the expression is as follows:

$$h = \frac{1}{\beta}\frac{u_*}{f}$$

where, β is an empirical parameter, generally taken as 6; f is the Coriolis force parameter, which is related to the latitude of the observation point, and is taken as 9.375×10^{-5}/s.

3.2. Time Characteristics of Measured Average Wind Speed and Wind Direction

Figure 3 shows the contours of the measured 10-min horizontal average wind speed and wind direction during the period from 8:00 on 9 August 2019, to 0:00 on 11 August 2019. The black dashed line in the figure indicates the time when the typhoon landed, which is 01:45 on 10 August 2019. Some white areas are caused by data exclusion. Figure 3a shows that the wind speed reached two peaks after the typhoon landed, forming a typical M shape structure. Moreover, the overall wind speed in the later stage of the measured typhoon is greater than that in the early stage. The maximum 10-min average wind speed in the later stage is 18 m/s, and the maximum instantaneous wind speed reaches 27.3 m/s. It is worth noting that there is an obvious low-level jet phenomenon within 150 m above

the ground. From 10:40 to 11:00 on August 10, the 10-min average wind speed at the lower level exceeded 12 m/s.
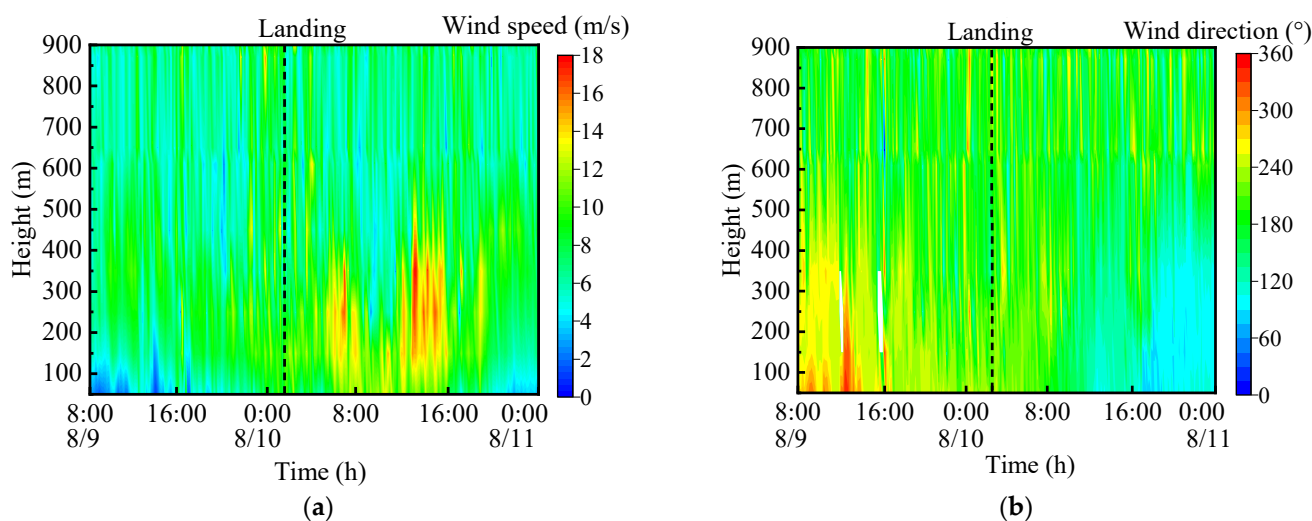

Figure 3. Measured 10-min horizontal wind speed and wind direction, including (**a**) Horizontal wind speed; (**b**) Horizontal wind direction; Time format: hh: mm/dd.

Figure 3b shows that during the passage of the typhoon, the average wind direction at the center of the measured points changed from southwest to southeast, and the average wind direction at 50 m changed by about 150°. The wind speed and direction changed significantly along the height direction. The measured height is below 550 m, and the wind speed increases significantly with the increase of height, with a significant change in wind direction; above 550 m, the changes in wind speed and direction with height and time are not significant. The wind speed gradually approaches consistency at different heights, and the change in wind direction angle is not significant, indicating that the gradient wind height has been reached.

4. Evolution Characteristics of Wind Profiles

4.1. Evolution of Typhoon Boundary Layer Wind Profile

The analysis of the evolution of the typhoon boundary layer wind profile from 8:00 on 9 August 2019, to 0:00 on 11 August 2019, based on the measured points within the influence range of the typhoon's 7th level wind circle, lasted a total of 40 h. Figures 4 and 5 show the evolution process of the measured boundary layer wind speed and wind direction profiles of typhoon Lekima, respectively. Each interval is divided based on 2 h, for a total of 20 intervals. Figure 4 also provides the extreme and peak values of the average wind speed span for each interval. The dotted line in the figure is the average wind speed profile in each interval, and the shaded part represents the peak of the horizontal average wind speed in this time interval. In Figure 5, the wind direction is 0° (360°) due north and 180° clockwise due south. The vertical height is 0 to 1000 m.

Intervals 6–8 (18:00 on the 9th to 0:00 on the 10th): As the distance between the typhoon center and the observation point decreases, the height of the maximum wind speed decreases from 300 m to 120 m, and the wind speed profile at the bottom shows anti-C shape; the horizontal average wind speed gradually increases, and the 10-min average wind speed below 500 m can reach 14 m/s. In Figure 5, the wind direction gradually rotated counterclockwise, the wind direction at the lower level was stable, and the wind direction above 750 m was relatively discrete.
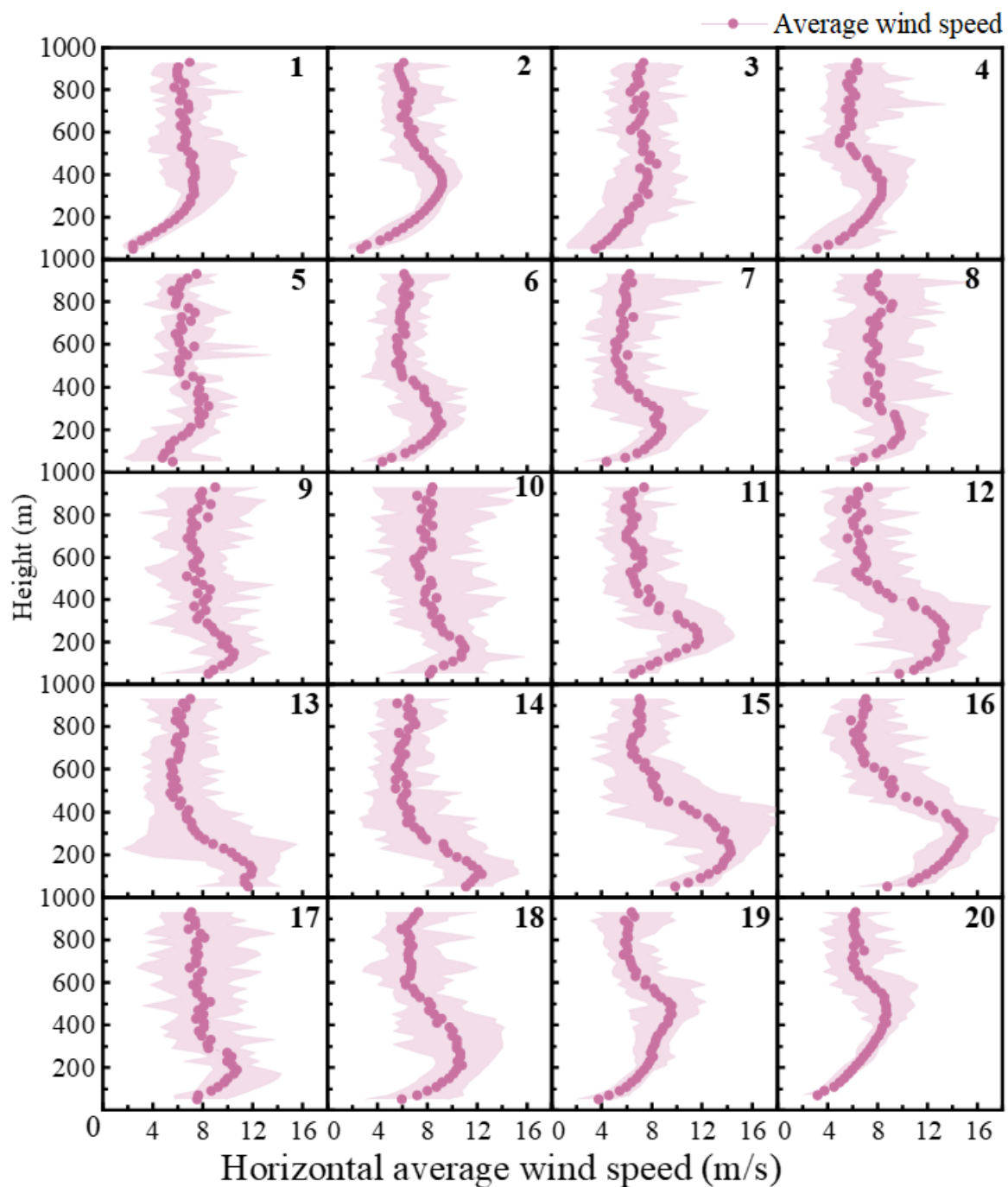
Figure 4. Evolution process of the boundary layer wind speed profile of typhoon Lekima.

Interval 9 (0:00 to 2:00 on the 10th): The typhoon makes landfall, and the measured point is affected by the 10-level wind circle.

Interval 10–16 (2:00 to 16:00 on the 10th): The distance between the measured point and the bottom center of the typhoon in interval 11 is the smallest, about 70.6 km. The wind speed above 800 m showed a trend of further increase during the interval between 11 and 12, but the second increase in wind speed did not surpass the lower-level extreme wind speed. In interval 14, the maximum horizontal average wind speed increases to about 14 m/s, appearing in the 120 m height layer, and the peak value of the 10-min average wind speed can reach 16 m/s. In Figure 5, when the typhoon center approaches and passes through the observation point, the wind direction changes significantly, and the change

becomes more intense with the increase in height. The wind profile shapes in intervals 11, 12, 15, and 16 are S shape.

Intervals 1–5 (8:00 to 18:00 on the 9th): The measured point is far away from the typhoon path. Starting from Interval 2, it is affected by the 7-level wind circle. From Figures 4 and 5, it can be seen that the wind speed and direction profile begin to change.
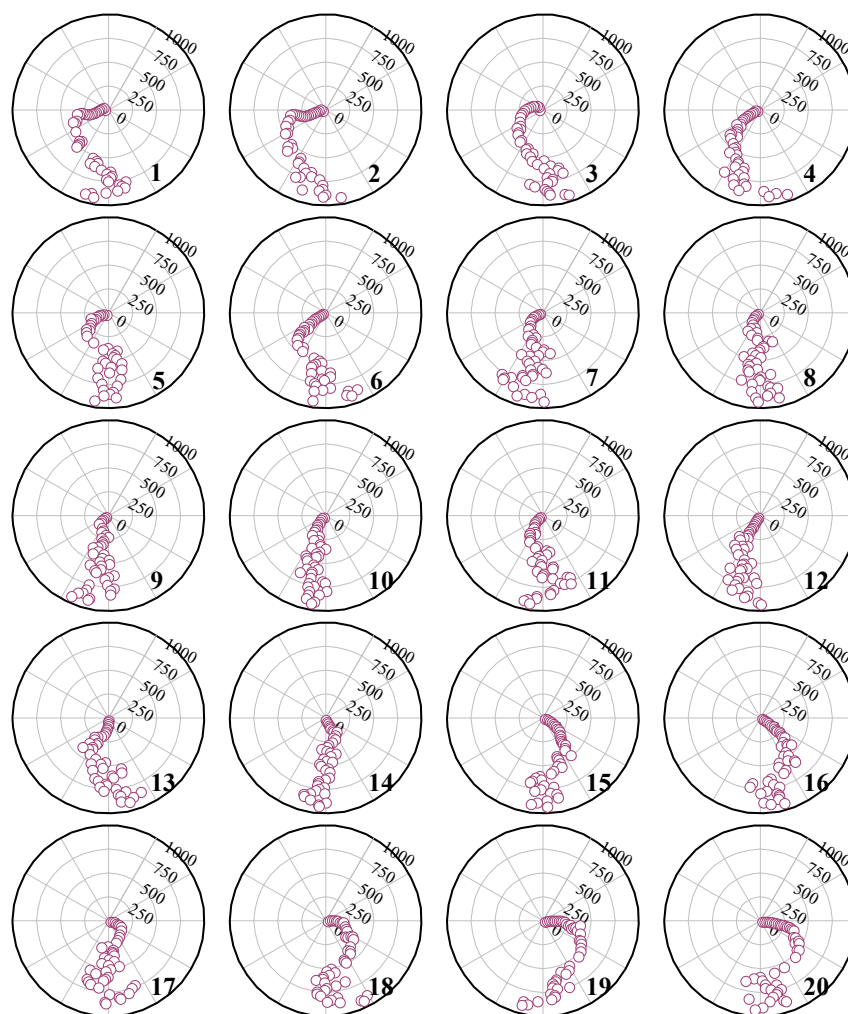

Figure 5. Evolution process of the boundary layer wind direction profile of typhoon Lekima.

During the process of a typhoon making landfall and moving inland, a significant low-level jet can be observed in the wind speed profile. The higher the average wind speed in the lower layer, the lower the height of the near-Earth jet layer. The height of the near-Earth jet layer refers to the altitude at which the low-level jet appears and is also the height of the low-level jet core (the apex of the "nose" profile). Kepert's research [36] indicates that the low-level jet is a common feature of the average wind profile in the boundary layer of tropical cyclones. Studies [9] have shown that the maximum average wind speed at the near-surface of Atlantic hurricanes is about 500–600 m vertical height, which is much higher than the maximum wind speed in this study. This may be related to the different ocean surfaces where the typhoon is generated. It is very unfavorable to the wind resistance of super high-rise structures in coastal areas.

Interval 17–20 (16:00 on the 10th to 0:00 on the 11th): The measured point gradually moves away from the typhoon and is still within the influence range of the 7-level wind circle. With the typhoon moving away and weakening, the wind speed at the bottom decreases, and the height of the maximum wind speed increases from 200 m to about 500 m.

In Figure 5, the wind direction changes completely, with a difference of about 180° from the initial wind direction.

In general, the characteristics of the typhoon boundary layer profile mainly have the following characteristics: (1) A low-level jet appears within the vertical height range of 120–500 m, with the maximum wind speed and a 180° change in wind direction. (2) The shape of the typhoon profile differs significantly from the theoretical profile model, depending on the radial position from the typhoon center to the outer edge of the typhoon.

4.2. Factors Affecting Wind Profiles

4.2.1. Influence of Typhoon Horizontal Structure on Wind Profile

Wind profile is the main factor affecting the wind load characteristics of high-rise buildings. To explore the influence of typhoon structure on the characteristics of wind profile, the wind profile of typhoons in different periods is discussed by time series. According to the evolution of the typhoon wind profile in Section 3.1, typhoons are divided into four periods, as shown in Table 2. They are the typhoon influence period, the typhoon landing period, the typhoon wind speed rising period, and the typhoon stable period.

Table 2. Different stages of typhoon.

Typhoon Stage Name	Corresponding Interval (NUM)	Wind Circle Range (Wind Scale)
Impact period	6–8, 17–18	7
Landing period	9	7–10
Wind speed rising period	10–12, 15–16	10
Stable period	13–14	7–10

Figure 6 shows the relationship between the maximum wind speed and the height of the maximum wind speed during the typhoon influence period and landing period with the distance (relative distance) between the measured ground and the typhoon center. According to the hour time path provided by the CMA, this is a total of 44. It can be seen that with the increase of relative distance, the maximum average wind speed gradually decreases, while the height of the maximum wind speed gradually increases, indicating that the greater the wind speed at the lower level, the lower the typhoon boundary layer and the more significant the low-level jet phenomenon.
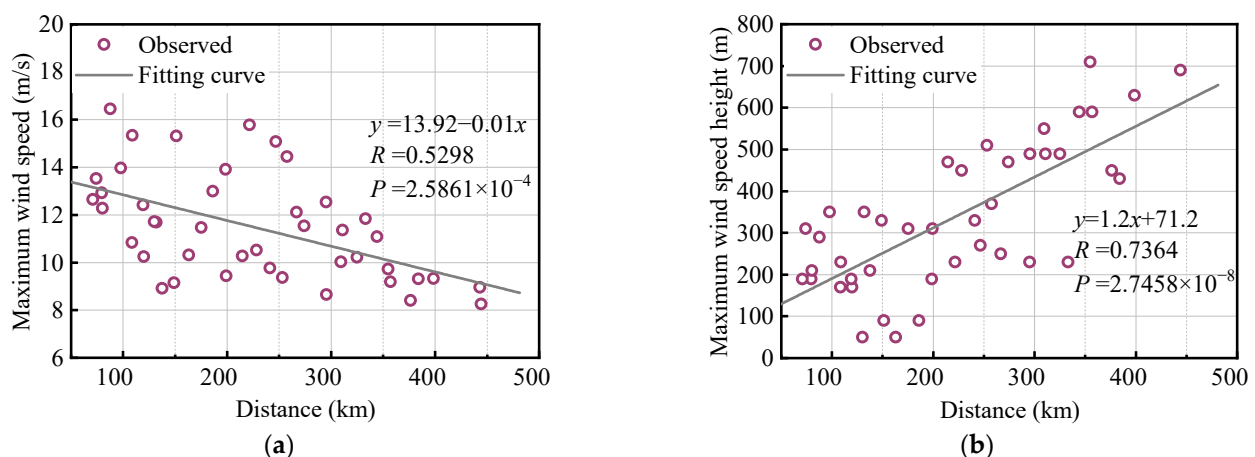

Figure 6. Changes of maximum wind speed and height of maximum wind speed with relative distance, including (**a**) maximum wind speed; (**b**) maximum wind speed height.

Figure 7 shows wind profiles during different periods of typhoons. The wind characteristics in different parts of a typhoon vary significantly. The typhoon influence period refers to the period when the typhoon approaches the coastline and moves away from the

observation point, both within the influence range of the 7-level wind circle. The observation point is far away from the bottom center of the typhoon, and the bottom wind speed is the smallest during this period. During the typhoon landing period, the observation points begin to be affected by the 10-level wind circle, the maximum wind speed height decreases, and the wind direction changes. The bottom wind speed rises sharply during the typhoon wind speed rise. In the stable period, the bottom wind speed is the largest and the maximum wind speed height is the lowest.
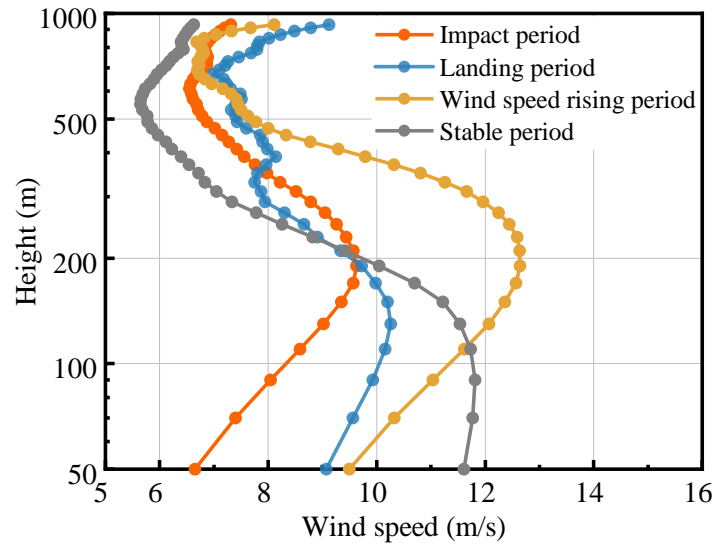

Figure 7. Wind profiles of different stages of typhoon.

Figure 8 compares the normalized average wind speed profiles with the empirical model for different stages of the typhoon. U_{50} represents the average wind speed at a vertical height of 50 meters. Considering the characteristics of the fitting model and combined with the characteristics of civil engineering structures, the measured data from the bottom to the height of the maximum wind speed or the wind speed with obvious inflection points in each period are fitted. The dynamic parameters such as wind profile index, roughness length, friction velocity, and boundary layer height are fitted, as shown in Table 3.

Table 3. Wind profile fitting parameters of typhoon at different stages.

Typhoon Period	Maximum Wind Speed Height (m)	Power-Law Model	Log-Law Model		D-H Model
		Index	Friction Velocity (m/s)	Roughness Length (m)	Boundary Layer Height (m)
Impact period	210	0.29	0.857	2.08	1524
Landing period	130	0.13	0.471	0.03	837
Wind speed rising period	210	0.23	0.917	0.739	1630
Stable period	110	0.04	0.182	0.01	324

Figure 8 shows that the three models can fit the wind profile from the ground to the height below the maximum wind speed well, but none of them can reproduce the anti-C shape wind profile and the phenomenon of secondary increase in wind speed. During the period of the typhoon's 7-level wind circle, the log-law and power-law fit the wind profile well at a height of 210 m. During the typhoon's landing period, the D-H model has the worst fitting effect. During the wind speed rising period, the three wind profile models can reflect the wind profile within 200 m near the ground. During the wind speed stable period, the normalized wind speed has an obvious inflection point at 110 m, and the wind

profile index is the smallest at this time. The typhoon wind profile shows a low-level jet near the ground, and the wind profile model may fail at heights above 200 m. This shows that the wind velocity profile below the height of the low-level jet follows the exponential law, logarithmic law, and D-H model, but the fitting parameters are greatly affected by the spatial position inside the typhoon wind field.
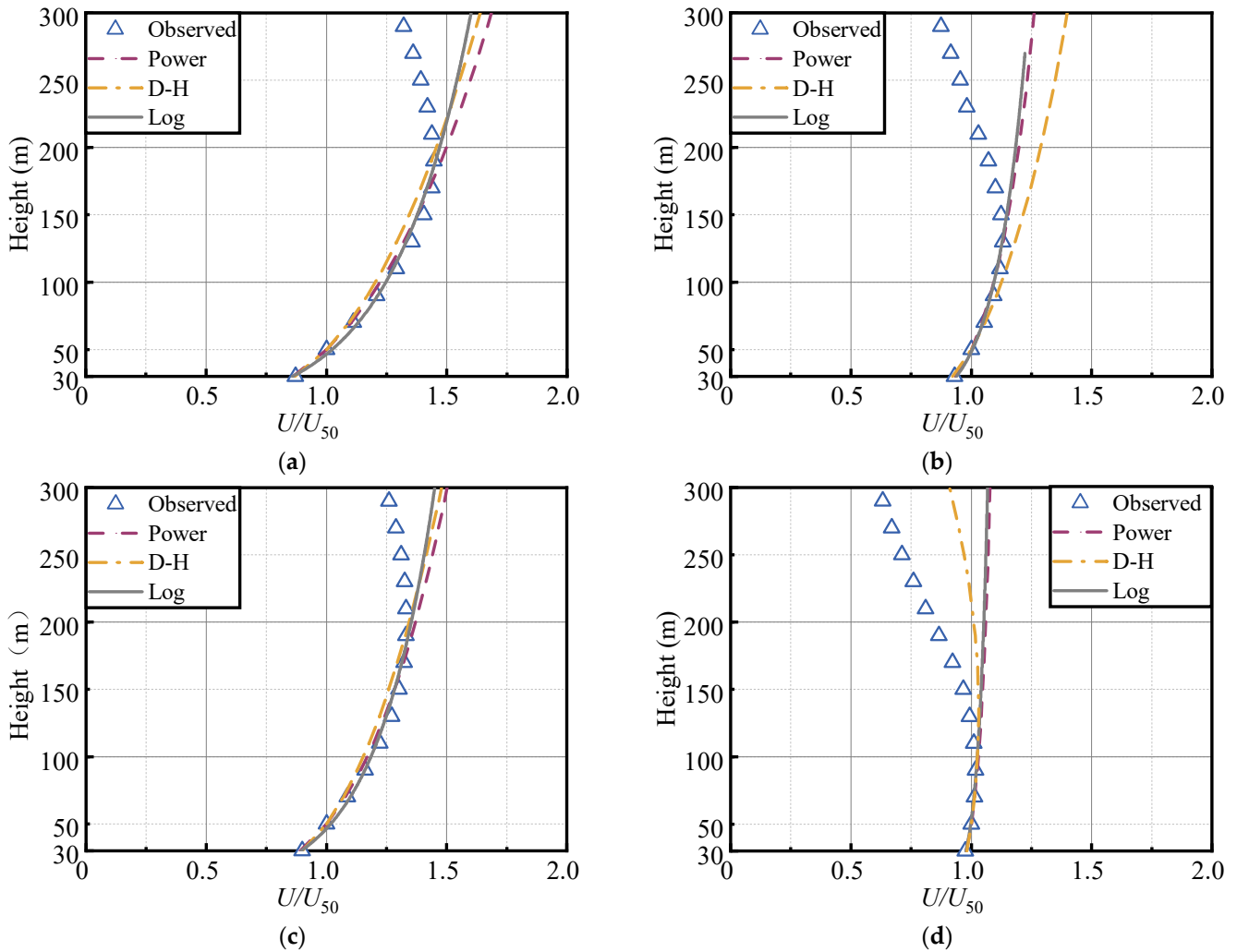

Figure 8. Comparison of wind profile models at different periods during typhoon Lekima, including (**a**) impact period; (**b**) landing period; (**c**) wind speed rising period; (**d**) stable period.

4.2.2. Influence of Incoming Wind Direction on Wind Profile

To study the influence of the average typhoon wind direction on the wind profile characteristics, the average wind speed at a height of 50 m (U_{50}) is used as the normalization to process the measured wind speed data at different heights with a basic time interval of 10 min. Considering the topographic effect near the observation point, the measured wind speed data at different heights are grouped based on the average wind direction at a height of 50 m. With a wind direction interval of $\theta = 45°$, the north direction is defined as $0°$ and divided into eight groups θ_i, i = 1, 2, 3, . . ., 8, which are $0°\sim45°$, $45°\sim90°$, $90°\sim135°$, . . ., $315°\sim360°$, respectively. To avoid the influence of the thermal effect, the wind data with wind speed less than 6 m/s are eliminated in the preprocessing of wind direction data. The average wind profile in each direction is shown in Figure 9. The missing wind direction intervals indicate that there is no data in that direction during the measurement period, or the data in that direction are removed because the wind speed at a height of 50 m is less than 6 m/s. The black squares in the figure represent the average wind speed records in

each direction interval at each height level, the red dots represent all the measured data at each height level in that direction interval, and the black horizontal bars are error bars, indicating the standard deviation of that layer. *N* represents the number of sets of measured data in that direction interval that meet the conditions.
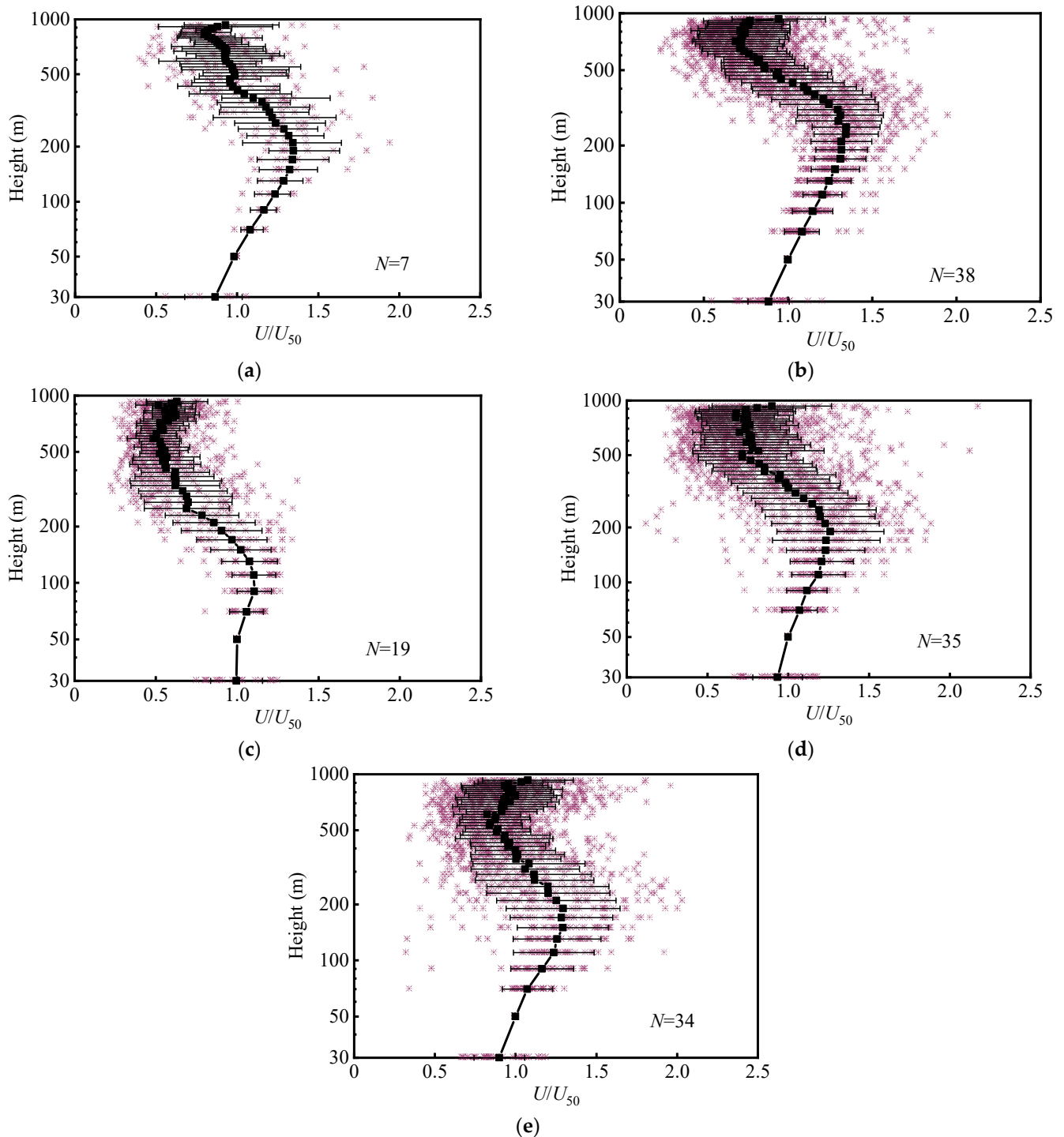

Figure 9. Wind profiles of typhoon Lekima in different average wind direction, including (**a**) *θ*2; (**b**) *θ*3; (**c**) *θ*4; (**d**) *θ*5; (**e**) *θ*6.

It can be seen from the wind direction grouping that there are obvious differences in the average wind speed profiles in different wind direction intervals, which is more apparent in the 500 m and above height layers. In *θ*2, the normalized wind speed at the

ground increases to 1.4 at the 200 m height layer, and then gradually decreases between 200–900 m height layers. For θ3 and θ4, an obvious acceleration effect can be observed in the wind speed profile at a height of about 600 m; that is, the normalized wind speed in the upper layer tends to increase again, showing an S shape profile, but the normalized wind speed increment does not exceed the extreme value of the bottom wind speed. In addition, the wind profile of θ4 at about 100 m height obviously deviates from the exponential or logarithmic profile, which may be due to the fact that the upwind direction of the measuring point is hilly terrain. For θ5 and θ6, the normalized wind speed continues to increase from the surface below about 200 m height, showing an exponential or logarithmic law of increase, and the normalized average wind speed value can reach about 1.3. There is a significant deceleration effect in the wind profile between 200–500 m. The normalized wind speed in the upper layer remains stable, indicating that it is not affected by the terrain.

4.2.3. Influence of Wind Speed on Wind Profile

In order to explore the influence of different wind speeds on wind profile characteristics, the wind profile during the typhoon measurement is grouped and integrated according to the wind speed at a height of 50 m, and the wind speed interval is 2 m/s, as shown in Figure 10.
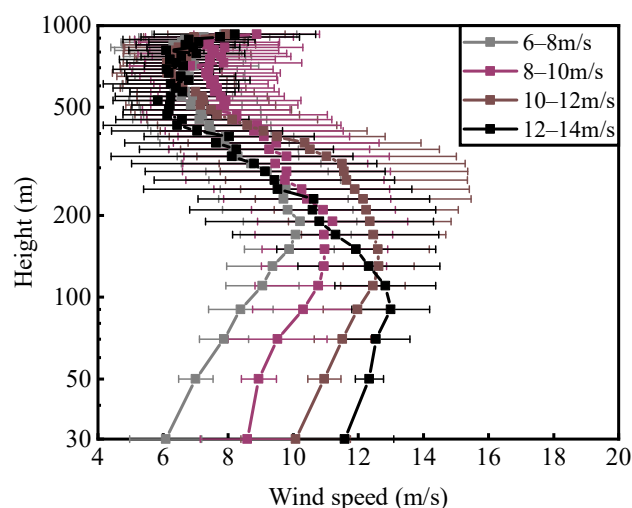

Figure 10. Wind profiles in different average wind speed intervals.

To avoid the influence of the thermal effect, data with wind speed of less than 6 m/s at a height of 50 m were also excluded. Based on the wind speed at the 50 m altitude level, the average wind speed profiles were divided into four groups: 6–8 m/s (46 profiles), 8–10 m/s (34 profiles), 10–12 m/s (37 profiles), and 12–14 m/s (16 profiles). The results show that the average wind velocity profile curve is different with different wind velocities, indicating that the average wind velocity profile curve is related to the wind velocity. The larger the wind speed range, the lower is the height of the maximum wind speed, the more drastic is the change of average wind speed with height, and the steeper is the wind profile curve. It is more obvious when the average wind speed is greater than 12 m/s. This is consistent with the conclusion of Powell [9] and Shu [37] in analyzing the typhoon wind profile. For a weather system with a larger average wind speed, the height of the maximum wind speed is lower.

4.2.4. Influence of Different Time Distance on Wind Profile

The average wind speed is calculated at intervals of 3 s, 10 min, and 1 h by engineering requirements or specification criteria. Different calculation results are obtained for the average wind speed at different intervals, leading to variations in the wind profile. Based

on the measured data of typhoon Lekima, the wind velocity profiles of short time (10 min) and long time (60 min) are compared.

Figure 11 shows the time history of the horizontal wind speed at different altitudes and different time distances. Part of the white space in the figure is caused by data quality control. From the wind speed time-history curve, it can be seen that with the increase of the average time interval, the average wind speed at heights of 600–1000 m decreases significantly. The larger the time interval, the gentler is the three-dimensional wind speed surface, indicating that the changing trend of the average wind speed with time interval becomes more stable. In the figure, the 10-min average wind speed time-history curve basically fluctuates around the 60-min time-history curve. Compared to the 10-min average wind speed interval, the 60-min average wind speed interval is no longer able to reflect the development trend of wind speeds at different heights during the passage of typhoons. Using a 10-min average wind speed interval to represent the intensity of the average wind is considered more reasonable by our country's standards.
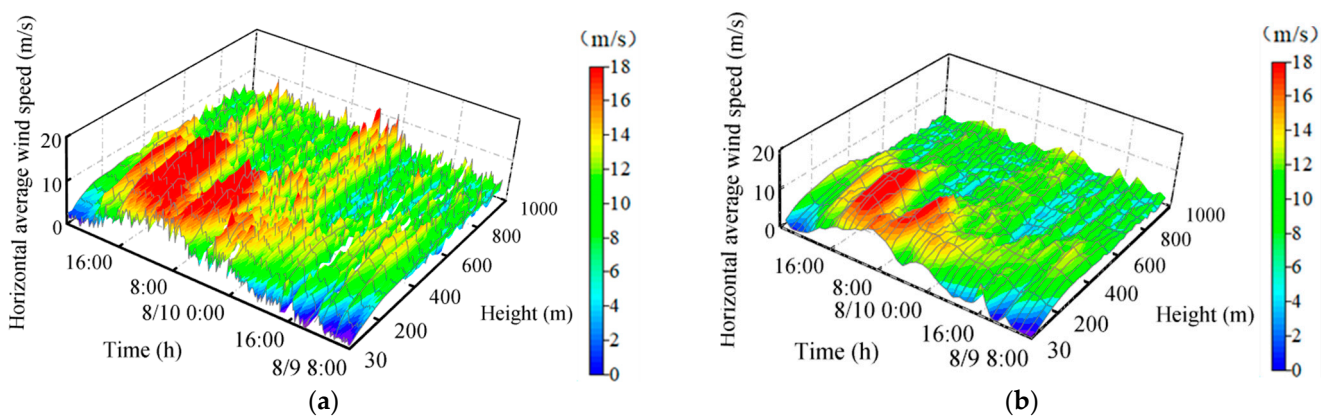

Figure 11. Horizontal wind speed time history at different time intervals, including (**a**) 10-min horizontal wind speed time history; (**b**) 60-min horizontal wind speed time history.

5. Evolution Characteristics of Wind Profile Parameters

5.1. Wind Profile Index

The vertical profile of the average wind speed within the boundary layer depends on a range of parameters, including upwind topography, surface roughness, atmospheric stability, and meantime distance. The wind profile index can reflect the variation of average wind speed with vertical height and is one of the important parameters for the wind resistance design of high-rise structures.

Figure 12 shows the change in typhoon wind profile index with 50 m average wind speed (0–5, 5–10, and 10–15 m/s) and vertical height (150 m and 250 m). In different height levels, the wind profile exponent tends to decrease as the average wind speed increases. Within the same wind speed group, the average wind profile exponent also decreases with increasing height. With the increase of U_{50}, the exponential distribution gradually changes from discrete to convergent. The wind profile exponent within the minimum wind speed range in the 150 m height level is 3.9 times that of the maximum wind speed range. In addition, the U_{50} is in the range of 10–15 m/s, and there is obviously a negative wind profile index, indicating that the wind profile distribution deviates from the power-law, log-law, and D-H model. There is a phenomenon of low-level jets.
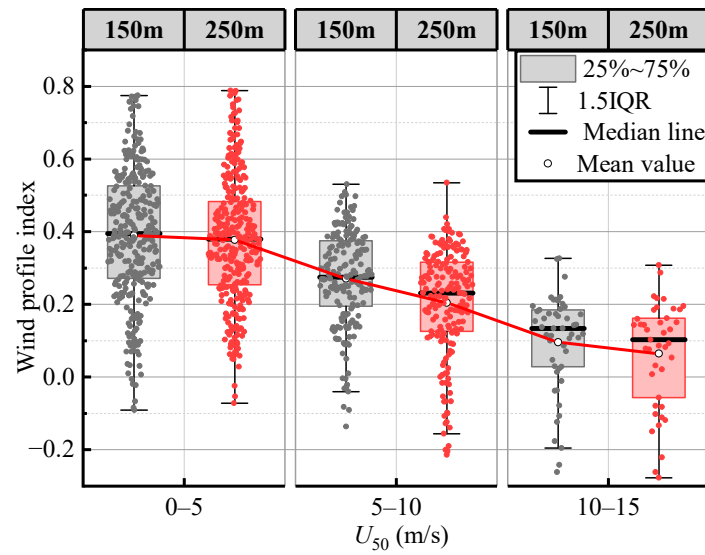
Figure 12. The change of wind profile index with average wind speed and height.

5.2. Roughness Length

The roughness length z_0 represents the roughness of the surface, and the greater the roughness length, the more obvious is the wind deceleration effect. Figure 13 shows the fitting comparison between the wind profile and the wind profile model of typhoon Lekima in different wind speed grades. The wind profile index, roughness length, and other parameters obtained by using the least square method [38] are listed in Table 4. R^2 represents the goodness of fit. The closer its value is to 1, the better the fitting degree. The fitting results show that the smaller the wind speed grade, the greater is the surface roughness length, which is consistent with the results of different impact stages of the typhoon. During the impact period of the typhoon's 7-level wind circle, the observation point is far away from the typhoon and is greatly affected by the terrain. When the average wind speed is greater than 12 m/s, the fitting effect of the wind profile model is the worst, which may be due to the small number of wind profile samples.
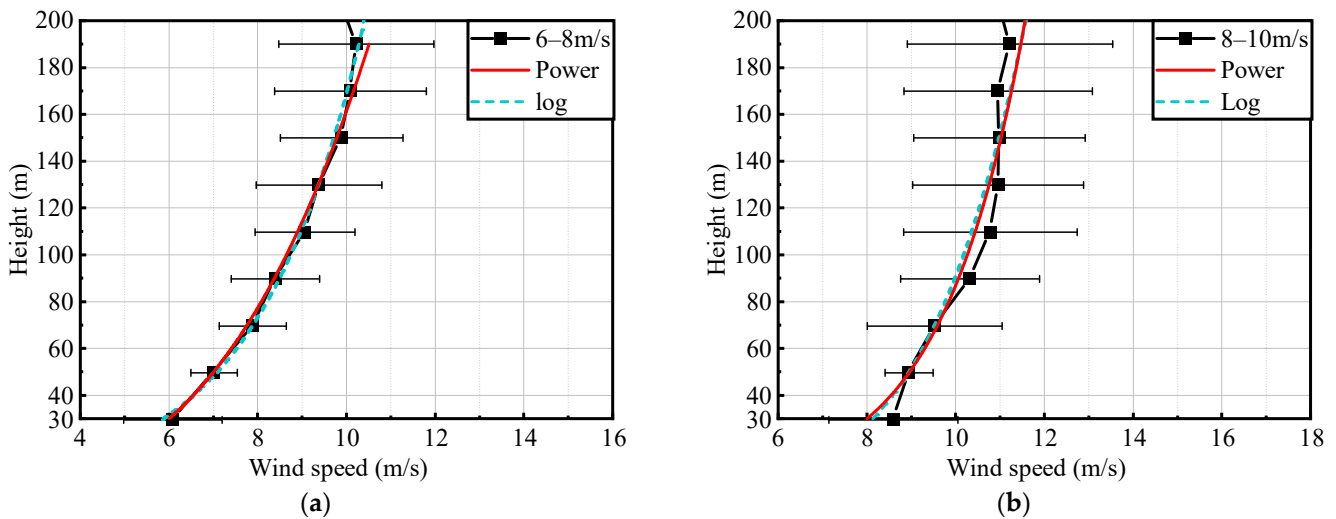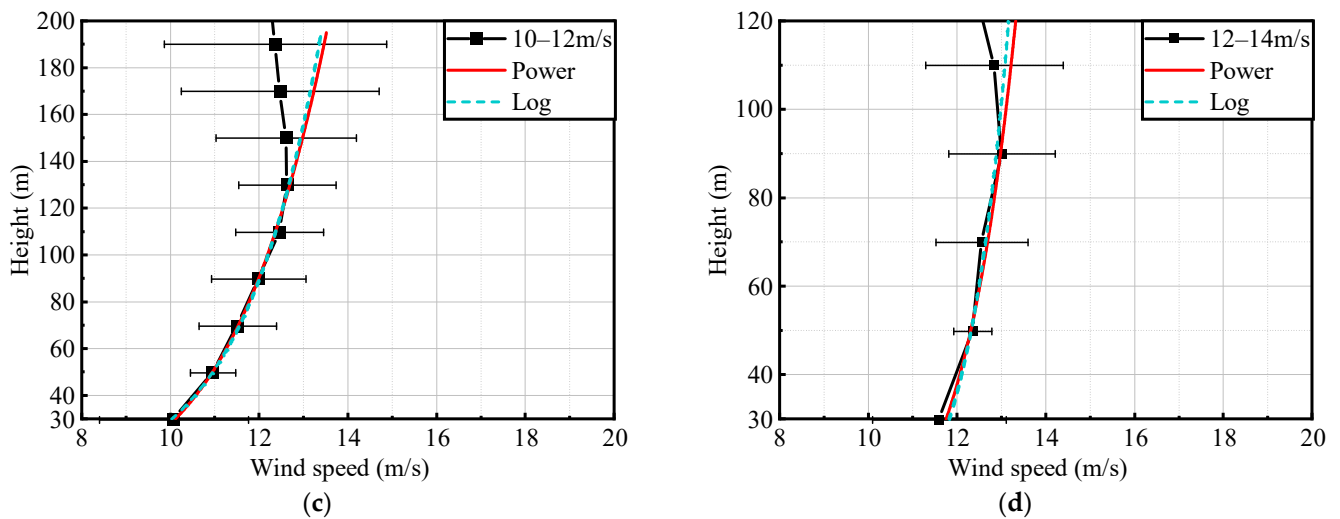

Figure 13. *Cont.*

Figure 13. Comparison of wind profile and fitting model of typhoon with different wind speed classes, including (**a**) $6 < U_{50} < 8$; (**b**) $8 < U_{50} < 10$; (**c**) $10 < U_{50} < 12$; (**d**) $12 < U_{50} < 14$.

Table 4. Wind profile fitting parameters of typhoon with different wind speed levels.

Wind Speed (m/s)	Sample Number N	Fitting Range (m)	Power-Law Model		Log-Law Model		
			Index	R^2	u_* (m/s)	z_0 (m/s)	R^2
6–8	46	30–190	0.3	0.994	0.958	2.607	0.993
8–10	34	30–150	0.186	0.944	0.774	0.489	0.974
10–12	37	30–130	0.155	0.997	0.716	0.111	0.997
12–14	16	30–110	0.091	0.938	0.385	3.82×10^{-4}	0.894

5.3. Boundary Layer Height and Maximum Wind Speed Height

The height of the atmospheric boundary layer refers to the height where the effect of surface friction can be ignored. Different countries' specifications provide suggested values based on the underlying terrain. However, existing research indicates that *h* is also influenced by factors such as the different stages of a typhoon and the average wind speed.

Based on Equation (5), it is calculated that the boundary layer height in the typhoon wind speed stable period is 324 m, which is slightly less than the boundary layer height of Class B terrain in the specification (350 m). During the impact period, landfall period, and wind speed rising period of the typhoon, the boundary layer heights are 1524 m, 837 m, and 1630 m, respectively. Compared with the specification, they increased by 335%, 139%, and 365%, respectively. This may be due to the small value of the specification. Zhang [39] obtained an average boundary layer height of 1421 m based on typhoon "Maria," which is 306% larger than the specification. The boundary layer height calculated by Li [40] measuring a super typhoon far exceeds the standard value.

6. Conclusions

Based on the field measured data of typhoon Lekima captured by wind profile acoustic radar, this paper systematically studied the global profile characteristics of the boundary layer of a super typhoon and deepened the understanding of the variability characteristics of the typhoon wind field in coastal areas. The main conclusions can be summarized as follows:

(1) The measured wind speed and wind direction profiles of typhoon Lekima showed strong variability. A low-level jet phenomenon existed near the vertical height of 0.12–0.5 km, and the maximum wind speed height varied with the evolution of the typhoon wind field. It is far lower than the approximate 500–600 m maximum wind speed height of the hurricane studied by Powell [9], which may be related to the

different ocean surface of typhoon generation. Below 500 m, the wind direction deflects 180°; however, above the altitude level of 500 m, the wind direction changes more violently with the increase of height, with great dispersion, which is mainly affected by the structure of the typhoon wind field.

(2) The evolution process of the typhoon wind velocity profile can be divided into four stages: influence period, landing period, wind velocity rising period, and stable period. The log-law, power-law, and D-H models can fit well the wind profile in the height range of 50–200 m. The "anti-C" wind profile and the "S" wind profile with secondary increase of wind speed cannot be reproduced. The "S" shape profile of secondary increase wind speed is less than the extreme wind speed at the bottom of the typhoon. In the wind resistance design of high-rise structures in coastal areas, the influence of extreme wind speed at the bottom of typhoon should be fully considered and evaluated.

(3) The measured typhoon wind profile is affected by many factors. When the wind direction is hilly, the wind profile in the jet layer will deviate from the theoretical model. The higher the wind speed, the lower is the maximum wind height, and the steeper is the wind profile curve. The larger the time interval, the smoother is the 3D surface of the average wind speed. The conversion of wind speed time interval should be avoided as far as possible in structural wind resistance design.

(4) Wind parameters are greatly affected by the spatial position inside the typhoon wind field. The wind profile index decreases with the increase of average wind speed and vertical height. With the increase of average wind speed, the index distribution of wind profile tends to converge from discrete. The smaller the range of wind speeds, the larger is the length of surface roughness z_0. Compared to the standard, the boundary layer height during the typhoon impact period, landing period, and wind speed increase period increased by 335%, 139%, and 365%, respectively.

Author Contributions: Conceptualization, Y.W.; methodology, Q.Q.; software, B.F.; validation, X.W.; formal analysis, B.F. and C.Z.; investigation, S.Z. and B.F.; resources, X.W.; data curation, L.Z. and M.Z.; writing—original draft preparation, B.F., Q.Q. and Y.W.; visualization, Y.W. All authors have read and agreed to the published version of the manuscript.

Institutional Review Board Statement: Not applicable.

Informed Consent Statement: Not applicable.

Data Availability Statement: The data presented in this study are available on request from the corresponding author.

Conflicts of Interest: The authors declare no conflicts of interest.

References

1. Fang, G.; Wei, M.; Zhao, L.; Xu, K.; Cao, S.; Ge, Y. Site-and building height-dependent design extreme wind speed vertical profile of tropical cyclone. *J. Build. Eng.* **2022**, *62*, 105322. [CrossRef]
2. Wang, Y.; Li, Y.; Qi, Q.; Zhang, C.; Wang, X.; Fan, G.; Fu, B. Experimental Study of the Fluctuating Wind Characteristics of Typhoon Jangmi Measured at the Top of a Building. *Sustainability* **2022**, *14*, 9266. [CrossRef]
3. Chen, T.; Fu, J.Y.; Chan, P.W.; He, Y.C.; Liu, A.M.; Zhou, W. Wind characteristics in typhoon boundary layer at coastal areas observed via a Lidar profiler. *J. Wind Eng. Ind. Aerodyn.* **2023**, *232*, 105253. [CrossRef]

4.　Fang, G.; Zhao, L.; Cao, S.; Zhu, L.; Ge, Y. Estimation of tropical cyclone wind hazards in coastal regions of China. *Nat. Hazards Earth Syst. Sci.* **2020**, *20*, 1617–1637. [CrossRef]

5.　Cheng, X.; Yan, B.; Zhou, X.; Yang, Q.; Huang, G.; Su, Y.; Yang, W.; Jiang, Y. Wind resource assessment at mountainous wind farm: Fusion of RANS and vertical multi-point on-site measured wind field data. *Appl. Energy* **2024**, *363*, 123116. [CrossRef]

6.　Yao, Y.; Wu, H.; Li, X.; Zhao, B.; Chen, B.; Yi, T. A review of the transmission tower-line system performance under typhoon in wind tunnel test. *Wind Struct.* **2019**, *29*, 87–98.

7.　Han, X.L.; Li, Q.S.; Zhou, K.; Li, M. Investigation of the Aerodynamic Forces on a 600-m-High Supertall Building by Field Measurements and Wind Tunnel Test. *J. Struct. Eng.* **2023**, *149*, 04023101. [CrossRef]

8.　Franklin, J.L.; Black, M.L.; Valde, K. GPS dropwindsonde wind profiles in hurricanes and their operational implications. *Weather Forecast.* **2003**, *18*, 32–44. [CrossRef]

9.　Powell, M.D.; Vickery, P.J.; Reinhold, T.A. Reduced drag coefficient for high wind speeds in tropical cyclones. *Nature* **2003**, *422*, 279–283. [CrossRef]

10.　Song, L.; Chen, W.; Wang, B.; Zhi, S.; Liu, A. Characteristics of wind profiles in the landfalling typhoon boundary layer. *J. Wind Eng. Ind. Aerodyn.* **2016**, *149*, 77–88. [CrossRef]

11.　Song, L.L.; Mao, H.Q.; Tang, H.Y.; Liu, A.J. Observation and Analysis of Guangdong Coastal Gales in the Near-surface Layer. *J. Trop. Meteorol.* **2004**, *20*, 731–736.

12.　Lin, L.; Chen, K.; Xia, D.; Wang, H.; Hu, H.; He, F. Analysis on the wind characteristics under typhoon climate at the southeast coast of China. *J. Wind Eng. Ind. Aerodyn.* **2018**, *182*, 37–48. [CrossRef]

13.　He, J.Y.; He, Y.C.; Li, Q.S.; Chan, P.W.; Zhang, L.; Yang, H.L.; Li, L. Observational study of wind characteristics, wind speed and turbulence profiles during Super Typhoon Mangkhut. *J. Wind Eng. Ind. Aerodyn.* **2020**, *206*, 104362. [CrossRef]

14.　Liu, Z.; Zheng, C.; Wu, Y.; Song, Y. Investigation on characteristics of thousand-meter height wind profiles at non-tropical cyclone prone areas based on field measurement. *Build. Environ.* **2018**, *130*, 62–73. [CrossRef]

15.　Zhuge, X.Y.; Guan, J.; Yu, F.; Wang, Y. A new satellite-based indicator for estimation of the western North Pacific tropical cyclone current intensity. *IEEE Trans. Geosci. Remote Sens.* **2015**, *53*, 5661–5676. [CrossRef]

16.　Wang, Y.; Xia, B.; Chen, Y.; Chen, H.; Xie, J. Revisiting the Characteristics of Super Typhoon Saola (2023) Using GPM, Himawari-9 and FY-4B Satellite Data. *Atmosphere* **2024**, *15*, 290. [CrossRef]

17.　Qi, W.; Yong, B.; Gourley, J.J. Monitoring the super typhoon lekima by GPM-based near-real-time satellite precipitation estimates. *J. Hydrol.* **2021**, *603*, 126968. [CrossRef]

18.　He, Y.; Chen, T.; Tang, J.; Chan, P.; Fu, J. Thermodynamic and Kinematic Structures in the Rainband Region of Typhoon Lekima (2019) at Landfall. *Atmosphere* **2022**, *13*, 312. [CrossRef]

19.　Lu, B.; Li, Q.S. Investigation of the effects of wind veering and low-level jet on wind loads of super high-rise buildings by large eddy simulations. *J. Wind Eng. Ind. Aerodyn.* **2022**, *227*, 105056. [CrossRef]

20.　Ren, H.; Laima, S.; Chen, W.-L.; Zhang, B.; Guo, A.; Li, H. Numerical simulation and prediction of spatial wind field under complex terrain. *J. Wind Eng. Ind. Aerodyn.* **2018**, *180*, 49–65. [CrossRef]

21.　Peng, S.; Liu, Y.; Li, R.; Wei, Y.; Chan, P.-W.; Li, S. Error Features in Predicting Typhoon Winds: A Case Study Comparing Simulated and Measured Data. *Atmosphere* **2022**, *13*, 158. [CrossRef]

22.　Mukherjee, P.; Ramakrishnan, B. Investigation of unique Arabian Sea tropical cyclone with GPU-based WRF model: A case study of Shaheen. *J. Atmos. Sol.-Terr. Phys.* **2023**, *246*, 106052. [CrossRef]

23.　Zhang, Y.; Cao, S.; Zhao, L.; Cao, J. A case application of WRF-UCM models to the simulation of urban wind speed profiles in a typhoon. *J. Wind Eng. Ind. Aerodyn.* **2022**, *220*, 104874. [CrossRef]

24.　Li, X.; Li, Y.; Zhou, J.; Wang, Q.; Wang, X. Characteristics of Typhoon "Fung-Wong" Near Earth Pulsation. *Shock Vib.* **2021**, *2021*, 9972981. [CrossRef]

25.　Liu, H.; He, M.; Wang, B.; Zhang, Q. Advances in low-level jet research and future prospects. *Acta Meteorologica Sinica* **2014**, *28*, 191–206. [CrossRef]

26.　Tao, T.; Wang, H.; Zhao, K. Efficient simulation of fully non-stationary random wind field based on reduced 2D hermite interpolation. *Mech. Syst. Signal Process.* **2021**, *150*, 107265. [CrossRef]

27.　Simiu, E.; Scanlan, R.H. *Effect of Wind on structure: An Introduction to Wind Engineering*; Tongji University Press: Shanghai, China, 1992.

28.　Monin, A.S.; Obukhov, A.M. Basic laws of turbulent mixing in the ground layer of the atmosphere. *Tr. Geofiz. Inst. Akad Nauk* **1954**, *24*, 163–187. Available online: https://scholar.google.com/scholar_lookup?title=Basic%20laws%20of%20turbulent%20mixing%20in%20the%20surface%20layer%20of%20the%20atmosphere&journal=Contrib%20Geophys%20Inst%20Acad%20Sci%20USSR&volume=151&issue=163&pages=163-187&publication_year=1954&author=Monin,A&author=Obukhov,A (accessed on 7 March 2024).

29.　Davenport, A.G. Rationale for determining design wind velocities. *J. Struct. Div.* **1960**, *126*, 39–68. [CrossRef]

30.　Wang, X.; Huang, P.; Gu, M. Field Measurements About Integral Scales of Near-ground Turbulence During Typhoon 'Muifa'. *J. Tongji Univ. Nat. Sci.* **2012**, *40*, 1491–1497.

31.　Wang, K.; Guo, Y.; Wang, X. Comparative Study of the Near-Surface Typhoon Wind Profile Fitting between Offshore and Onshore Areas. *Math. Probl. Eng.* **2021**, *2021*, 7422926. [CrossRef]

32.　*G.B. 50009-2012*; Load Code for the Design of Building Structures. China Architecture and Building Press: Beijing, China, 2012.

33. ASCE. Minimum Design Loads for Buildings and Other Structures (ASCE/SEI 7-10). *Am. Soc. Civ. Eng.* **2014**, *559*, 996.
34. Architectural Institute of Japan. *AIJ2004 Recommendations for Loads on Buildings*; Architectural Institute of Japan: Tokyo, Japan, 2004.
35. Deaves, D.M.; Harris, R.I. *A Mathematical Model of the Structure of Strong Winds*; Construction Industry Research and Information Association: London, UK, 1978.
36. Kepert, J.; Wang, Y. The dynamics of boundary layer jets within the tropical cyclone core. Part II: Nonlinear Enhancement. *J. Atmos. Sci.* **2001**, *58*, 2485–2501.
37. Shu, Z.R.; Li, Q.S.; He, Y.C.; Chan, P.W. Vertical wind profiles for typhoon, monsoon and thunderstorm winds. *J. Wind Eng. Ind. Aerodyn.* **2017**, *168*, 190–199. [CrossRef]
38. Yao, J.W.; Hang, C.Y.; Zhuang, Z.; Liu, J.T.; Ban, Q.C. Study on Precise calculation method of urban surface roughness parameters in numerical simulation of urban ventilation. *Build. Sci.* **2020**, *36*, 99–106.
39. Chuanxiong, Z.; Yanru, W.; Zhangqi, H. Field measurement study on wind structure characteristics of specific topography under typhoon Maria. *J. Nat. Disasters* **2019**, *28*, 100–110.
40. Li, Q.S.; Zhi, L.; Hu, F. Field monitoring of boundary layer wind characteristics in urban area. *Wind Struct.* **2009**, *12*, 553–574. [CrossRef]